

# OPTIMISED GETTERING AND HYDROGENATION OF MULTI-CRYSTALLINE SILICON WAFERS FOR USE IN SOLAR CELLS

J. Tan<sup>1</sup>, A. Cuevas<sup>1</sup>, D. Macdonald<sup>1</sup>, N. Bennett<sup>1</sup>, I. Romijn<sup>2</sup>, T. Trupke<sup>3</sup>, R. Bardos<sup>3</sup>

<sup>1</sup>College of Engineering and Computer Science, The Australian National University, Canberra, ACT 0200, Australia

<sup>2</sup>ECN Solar Energy, PO Box 1, Westerduinweg 3, NL 1755 ZG Petten, The Netherlands

<sup>3</sup>Centre of Excellence for Advanced Silicon Photovoltaics and Photonics, University of New South Wales, Sydney, 2052, Australia

**ABSTRACT:** In this paper, two types of phosphorus gettering have been compared. In addition, two annealing conditions for high density PECVD silicon nitride films are investigated. Our results show that optimised gettering and SiN induced hydrogenation can reduce and maintain interstitial iron concentrations  $\leq 10^{10}$  Atoms/cm<sup>3</sup>, as well as reducing the recombination strength of lattice dislocations. However, non ideal SiN annealing conditions can dissolve metal precipitates, resulting in high interstitial Fe concentrations as well as allowing passivated lattice dislocations to regain recombination strength.

**Keywords:** Gettering, Passivation, Degradation, Multi-crystalline

## 1 INTRODUCTION

Most solar cells today are produced with a multi-crystalline silicon (mc-Si) substrate. This substrate is inherently defect and impurity rich.[1,2] This work investigates what impacts phosphorus gettering and SiN induced hydrogenation have on a variety of physical and electronic properties of the mc-Si wafer. Three characteristics were studied as a function of brick position; minority carrier lifetime, interstitial iron concentration and the components of the relative recombination rate. Photoluminescence imaging has been employed to give a spatially resolved understanding of the changes that these processes induce.

## 2 EXPERIMENTAL DETAILS

A 125x125mm<sup>2</sup> *p*-type 1.6Ωcm (nominal) mc-Si brick was divided into six evenly spaced groups of wafers. Adjacent wafers from these sections were sorted into 5 sets of samples. The first series of wafers were alkaline then acid etched, and set aside as controls. These wafers will hence be referred to as “As-Cut”. The next set of wafers received an alkaline etch prior to a double sided “Standard” phosphorus diffusion. The remaining three sets of wafers were processed with “Extended” phosphorus diffusions.[3,4] Both recipes created sheet resistances of  $\sim 75\Omega/\square$ . The two diffusion recipes are



Figure 1 - Phosphorus gettering recipe.

shown in Fig. 1. All wafers were then coated (double-sided) in a dense SiN film. Details about the film deposited and the reactor used, can be found in references [5] and [6] respectively.

After SiN deposition, two sets of “Extended” gettered wafers were ‘fired’ in a Unitemp UTP-1100 rapid thermal processing furnace. One set of wafers were annealed at 800°C for 3s, the other at 800°C for 300s. Anneals were conducted in a N<sub>2</sub> ambient.

Annealed wafers were then stripped of their fired SiN films, acid etched to remove the n<sup>+</sup> emitters and re-passivated with a fresh SiN. All wafers were then forming gas annealed to further suppress surface recombination.

The photoconductance was measured at nine separate points across the sample using QSSPC.[7] Three parameters were studied: effective lifetime ( $\tau_{\text{eff}}$ ), interstitial iron concentration [Fe<sub>i</sub>] [8,9] and the components of the relative recombination rate.  $\tau_{\text{eff}}$  were compared at an excess carrier concentration of  $1 \times 10^{15} \text{cm}^{-3}$ . Photoluminescence (PL) images of the samples were taken under  $\sim 0.7$ Suns illumination intensity, with a constant 1s exposure time.[10]

To test that furnace contamination did not affect our results, 1Ωcm *p*-type <100> Float Zone wafers coated in the same SiN, were also annealed at 800°C for 300s. A very minor increase in [Fe<sub>i</sub>] was detected in these samples after annealing ( $\sim 1 \times 10^{10} \rightarrow 5 \times 10^{10} \text{Atoms/cm}^3$ ), reflecting the efficacy of the SiN film as a diffusion barrier to external contamination. Therefore, [Fe<sub>i</sub>]  $> 5 \times 10^{10} \text{Atoms/cm}^3$  in the mc-Si wafers after annealing must be due to a contamination source *internal* to the wafer.

## 3 AS-CUT WAFERS

Fig. 2(a) shows that the  $\tau_{\text{eff}}$  of the mc-Si brick varies greatly with position. One of the main factors responsible for the fluctuating  $\tau_{\text{eff}}$  is [Fe<sub>i</sub>], which is depicted in Fig. 2(b). High [Fe<sub>i</sub>] observed at the top and bottom of the brick are caused by the segregation of impurities in the Si melt and the diffusion of impurities into the Si from the crucible respectively.[11] Interestingly, [Fe<sub>i</sub>] observed at the *very* bottom of the brick are *lower* than what is observed at the next nearest region. This counter-intuitive

trend was investigated with PL imaging.

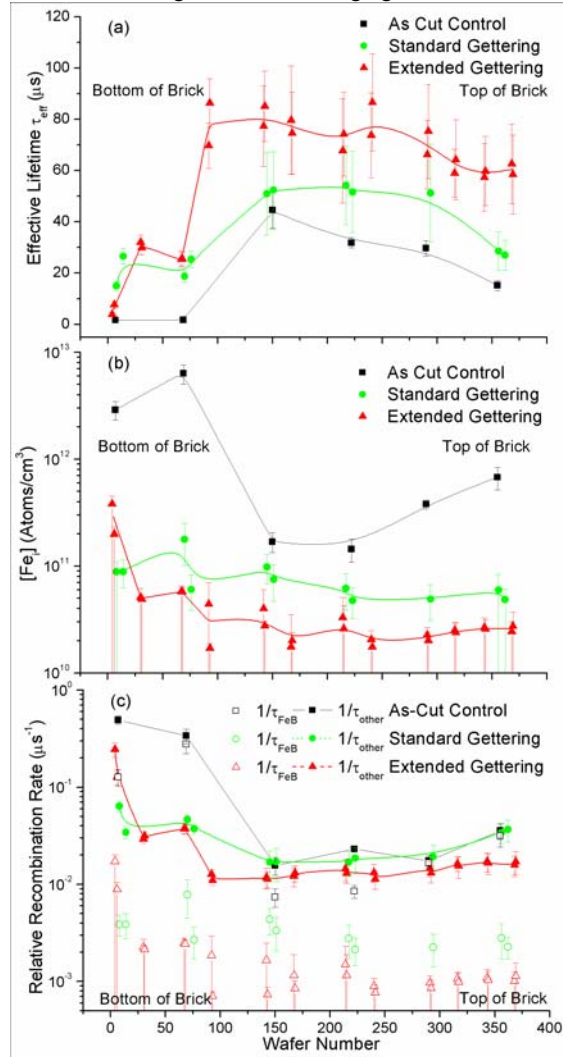


Figure 2 – (a)  $\tau_{\text{eff}}$ , (b)  $[\text{Fe}_i]$  and (c) components of the recombination rate, for as-cut and gettered wafers as a function of position along the mc-Si brick. Error bars represent the standard deviation of results. Negative error bars extending to zero indicate a detection limited result. Lines are a guide for the eye.

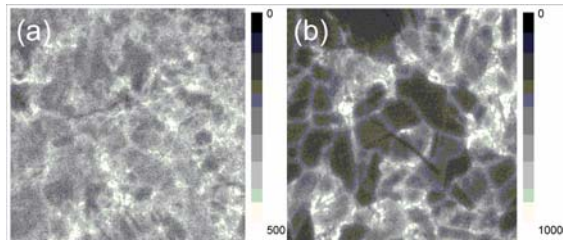


Figure 3 – Magnified photoluminescence images of as-cut wafers from the very bottom (a) and near bottom (b) regions of the mc-Si brick. Colour bars are linearly scaled.

Fig. 3 displays magnified PL images of as-cut wafers sampled from the two lowest regions of the mc-Si brick. When examining these images, one should note that the range of the colour bar of Fig. 3(a) is half that of Fig. 3(b). Both images in Fig. 3 reveal that the *highest* PL

count rates of highly contaminated wafers is found in regions surrounding lattice dislocations and grain boundaries. The fundamental cause of this phenomenon is the diffusion and precipitation of impurities immediately surrounding extended defects during the last stages of ingot cool down. Crystal defects allow easy precipitation of interstitial impurities. During the last stages of ingot solidification, impurities situated close to lattice defects are still mobile enough to diffuse to these sites and precipitate. As more impurities precipitate, regions surrounding lattice dislocations and grain boundaries become “denuded” of impurities. These areas of lower impurity concentration display higher PL count rates than more heavily contaminated regions in the crystals. As wafers from the very bottom of the brick have the smallest grain sizes, large areas of the wafers allow easy precipitation of interstitial impurities.[2] This explains why wafers from the very bottom of the brick can have *lower interstitial iron concentrations* than wafers sourced from deeper in the brick.

### 3 PHOSPHORUS GETTERED WAFERS

Fig. 2(a) clearly shows that phosphorus gettering is able to improve the  $\tau_{\text{eff}}$  of wafers across the mc-Si brick. For the majority of the brick, the ‘extended’ gettering process was able to further improve upon the  $\tau_{\text{eff}}$  achieved by ‘standard’ gettering. This is most notable at the top of the brick, where the ‘extended’ gettering process was able to stop the degradation of  $\tau_{\text{eff}}$  observed in as-cut and ‘standard’ gettered wafers. However, for wafers from the bottom two sections of the brick, both gettering regimes produced similar results. Fig. 2(b) and 2(c) depict factors which influence the  $\tau_{\text{eff}}$  results observed in Fig. 2(a).

#### 3.1 Impact of phosphorus gettering on $[\text{Fe}_i]$

Interestingly, Fig. 2(b) demonstrates that the ‘standard’ gettering process has reduced  $[\text{Fe}_i]$  of *all* regions of the mc-Si brick to  $\sim 10^{11}$  Atoms/cm<sup>3</sup>. As gettering of  $\text{Fe}_i$  and dissolution of Fe precipitates occurs simultaneously at high temperatures [12], the two mechanisms must have settled to a steady-state balance by the conclusion of the ‘standard’ gettering process.

In contrast, the extended gettering process was able to reduce the  $[\text{Fe}_i]$  of wafers from all regions of the brick below the detection limit of the technique. This demonstrates that the 600°C ‘tail’ of the extended gettering process was effective at neutralizing  $\text{Fe}_i$  while preventing further dissolution of Fe precipitates. From these results, it is not possible to determine whether the detection limited  $[\text{Fe}_i]$  were caused by the additional time allowed for  $\text{Fe}_i$  to diffuse to a gettering site, or heterogeneous precipitation [13] due to the low solid solubility of  $\text{Fe}_i$  in Si at 600°C.[14]

#### 3.2 Impact of gettering on the components of the relative recombination rate.

As displayed in Fig. 2(c), the total recombination rate ( $\tau_{\text{eff}}^{-1}$ ) of mc-Si wafers can be broken down into components.  $\tau_{\text{FeB}}^{-1}$  represents the relative recombination due to Fe-B pairs, the form  $\text{Fe}_i$  takes prior to illumination.  $\tau_{\text{other}}^{-1}$  represents the relative recombination rate due to all other sources. In mc-Si wafers this could include recombination via lattice dislocations, grain boundaries, impurities other than  $\text{Fe}_i$  and surface recombination. As the wafers received the same etching

and passivation treatments, the surface recombination velocity of all wafers should be low and comparable.

Fig. 2(c) shows that the low  $[Fe_i]$  observed after getting (Fig. 2(b)), have translated into very low rates of recombination via Fe-B pairs. As  $\tau_{FeB}^{-1} \ll \tau_{other}^{-1}$ ,  $\tau_{eff}^{-1}$  is dominated by  $\tau_{other}^{-1}$ .

Ignoring the results of wafer numbers <10 (which are skewed by the fast changing crystal structures found close to the ‘seed’ point), both getting treatments have reduced  $\tau_{other}^{-1}$  of wafers 25-90 to the same level. This level is likely the limit imposed by non-getter-able impurities and crystallography, and is reflected in the similar  $\tau_{eff}$  results of gettered wafers from the bottom two regions of the brick (Fig. 2(a)).

Considering the overlapping error bars of wafers 100 to 300,  $\tau_{other}^{-1}$  of all these wafers are essentially the same regardless of the getting regime. As impurity concentrations are typically the lowest in these regions of the mc-Si brick [1],  $\tau_{other}^{-1}$  primarily reflects the limit imposed by the crystallography. Therefore, as ‘extended’ getting was able to further improve upon the  $\tau_{eff}$  achieved by ‘standard’ getting from these wafers (Fig. 2(a)), the higher  $\tau_{eff}$  produced by ‘extended’ getting must reflect the complete removal of  $Fe_i$  from the bulk of these wafers.

Fig. 2(c) shows that the  $\tau_{other}^{-1}$  results of as-cut and ‘standard’ gettered wafers from the top of the brick are identical. In contrast,  $\tau_{other}^{-1}$  of ‘extended’ gettered wafers is noticeably lower. Therefore the ‘extended’ getting regime was able to neutralize an impurity that ‘standard’ getting was unable to affect. As the ‘tail’ of the ‘extended’ getting profile was optimized to get  $Fe_i$  [14], the impurity neutralized in these wafers must have a diffusivity comparable to  $Fe_i$ . Chromium is a likely candidate, as it is a known lifetime killer, can be phosphorus gettered, has a diffusivity slightly lower than  $Fe_i$  and is known to exist in mc-Si bricks.[15]

#### 4 GETTERED AND HYDROGENATED WAFERS

Previous work has shown that annealing SiN coated mc-Si wafers can increase their  $\tau_{eff}$ . [5,16,17] Fig. 4 demonstrates the impact of the two SiN annealing conditions on ‘extended’ gettered wafers, as a function of brick position.

Fig. 4(a) reveals that annealing conditions have a strong impact on the  $\tau_{eff}$  of SiN coated mc-Si wafers. The 800°C 3s anneal has improved the area averaged  $\tau_{eff}$  of most sections of the brick. In contrast, the 800°C 300s anneal has reduced the  $\tau_{eff}$  of most wafers below that achieved by ‘extended’ getting. Figs. 4(b) and (c) show the factors influencing the results displayed in Fig. 4(a).

##### 4.1 SiN annealing conditions impact on $[Fe_i]$

As previously observed in Fig. 2(b), extended getting results in  $[Fe_i]$  below the detection limit of the technique. Therefore significant  $[Fe_i]$  detected after annealing must be caused by the dissolution of Fe precipitates.[12] Fig. 4(b) shows that all wafers annealed at 800°C for 3s have very low  $[Fe_i]$ . In contrast, some wafers annealed at 800°C for 300s have very high  $[Fe_i]$ . Therefore SiN anneal conditions can have a strong impact on the  $[Fe_i]$  of well gettered mc-Si wafers.

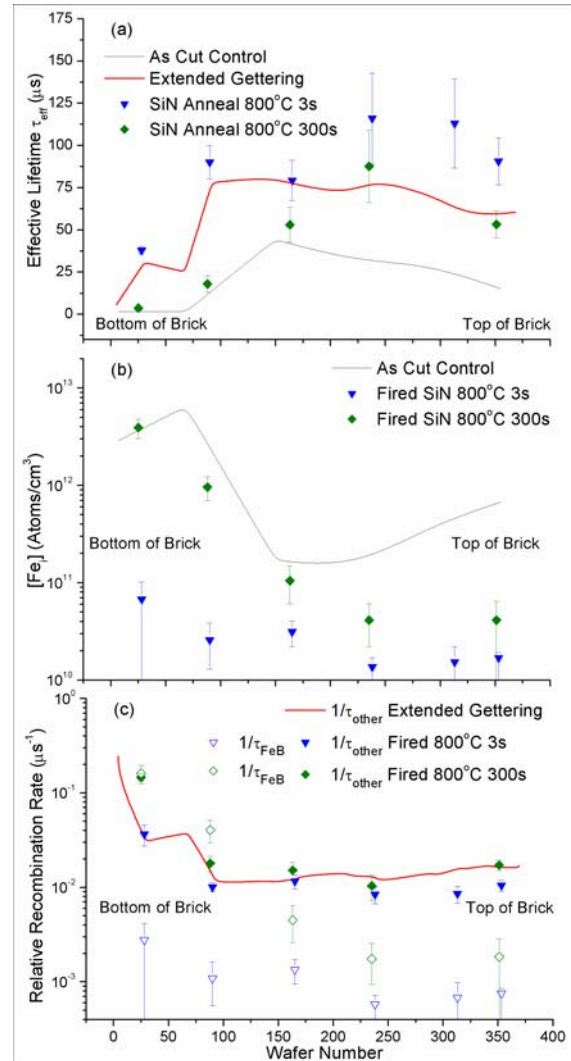


Figure 4 - (a)  $\tau_{eff}$ , (b)  $[Fe_i]$  and (c) components of the recombination rate, for as-cut and gettered wafers as a function of position along the mc-Si brick. Error bars represent the standard deviation of results. Negative error bars extending to zero indicate a detection limited result. Lines are a guide for the eye.

The  $[Fe_i]$  of wafers annealed at 800°C for 300s are strongly influenced by brick position. Wafers from the bottom two sections of the brick reveal high  $[Fe_i]$  after the 300s anneal. Meanwhile wafers from the top half of the brick have low  $[Fe_i]$  after the same anneal. This ‘asymmetric’ result is interesting as Macdonald *et al.* [1] have shown that Fe precipitate concentrations at the top and bottom of non-processed mc-Si bricks are similar.

Two explanations could explain this result. The first is that the most highly contaminated top regions of the brick were removed and recycled prior to wafering, and were hence not tested. The second explanation is that the chemical state of Fe precipitates varies across the brick, and Fe precipitates at the top of the brick are not as easily dissolved as those at the bottom of the brick.  $FeSi_2$  are known to form two chemical states.  $\alpha$ - $FeSi_2$  are known to be stable up to 1210°C.  $\beta$ - $FeSi_2$  though, have been shown

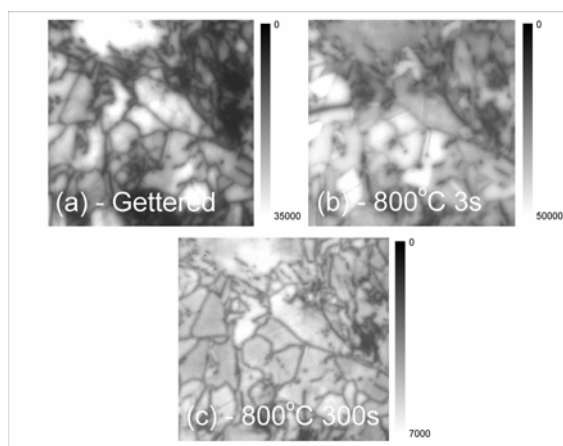


Figure 5 – Magnified photoluminescence images of wafers from the near bottom of the brick. (a) Extended Gettered, (b) Hydrogenated 800C 3s, (c) Hydrogenated 800C 300s. Colour bars are linearly scaled.

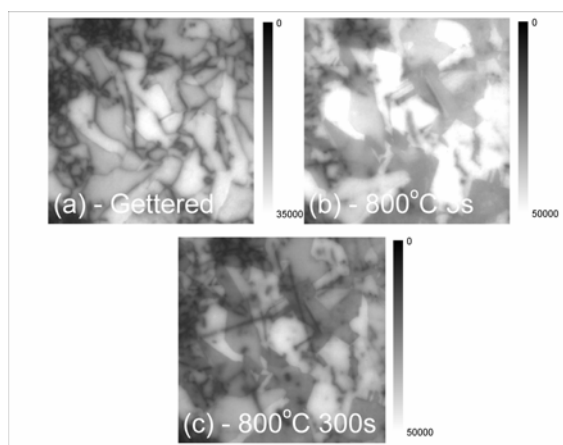


Figure 6 - Magnified photoluminescence images of wafers from the very top of the brick. (a) Extended Gettered, (b) Hydrogenated 800C 3s, (c) Hydrogenated 800C 300s. Colour bars are linearly scaled.

to be dissolved at temperatures  $>760^{\circ}\text{C}$ . [12] In addition,  $\alpha\text{-FeSi}_2$  are known to convert to  $\beta\text{-FeSi}_2$  at temperatures  $>915^{\circ}\text{C}$ . As the bottom of the mc-Si brick cools very slowly, a large percentage of the  $\text{FeSi}_2$  population in the bottom of the brick are likely in the  $\beta$  form. In contrast, the faster cooling rates at the top of the mc-Si brick may prevent the evolution of  $\alpha\text{-FeSi}_2$  into  $\beta\text{-FeSi}_2$ . Therefore wafers from the bottom of the brick are the most likely to record a high  $[\text{Fe}_i]$  after long anneals at temperatures  $>760^{\circ}\text{C}$ . [12].

#### 4.2 SiN annealing conditions impact on components of the relative recombination rate

Fig. 4(c) shows that  $\tau_{\text{FeB}}^{-1} \ll \tau_{\text{other}}^{-1}$  in wafers annealed at  $800^{\circ}\text{C}$  for 3s. It is also clear that the  $\tau_{\text{other}}^{-1}$  of these wafers are lower than  $\tau_{\text{other}}^{-1}$  of extended gettered wafers. Therefore, the increased  $\tau_{\text{eff}}$  observed in wafers annealed at  $800^{\circ}\text{C}$  for 3s (Fig. 4(a)) is primarily caused by the reduction of  $\tau_{\text{other}}^{-1}$ . Inspection of the PL images displayed in Figs. 5 and 6 reveal the source of the reduced  $\tau_{\text{other}}^{-1}$ .

Figs. 5 and 6 display PL images of wafers after SiN annealing. One should note the varying range of the colour bars when comparing the images. From the (a)

and (b) images of Figs. 5 and Figs. 6, we can observe that SiN induced hydrogenation has reduced the recombination strength of grain boundaries and dislocation clusters. This is similar to what other researchers have observed using different techniques. [18,19] Therefore the passivation of lattice dislocations and grain boundaries is the major factor behind the reduced  $\tau_{\text{other}}^{-1}$  of wafers annealed at  $800^{\circ}\text{C}$  for 3s.

Inspecting the results of wafers annealed at  $800^{\circ}\text{C}$  for 300s, displayed in Fig. 4(c), reveals:

1.  $\tau_{\text{FeB}}^{-1}$  has increased significantly in wafers known to have high  $[\text{Fe}_i]$  after annealing.
2. in re-contaminated wafers,  $\tau_{\text{FeB}}^{-1}$  is often equal to or greater than  $\tau_{\text{other}}^{-1}$ .
3.  $\tau_{\text{other}}^{-1}$  of most wafers have degraded from what was observed after ‘extended’ gettering.
4. degradation of  $\tau_{\text{other}}^{-1}$  is strongly influenced by brick position.

All these results are reflected in the PL images of Figs. 5 and 6. The low PL counts rates of intra-grain regions in Fig. 5(c) are likely caused by the high  $\tau_{\text{FeB}}^{-1}$  in this wafer. The fact that the crystals are homogeneously poor indicates that heterogeneously nucleated precipitates were dissolved. Fig. 5(c) also shows that lattice dislocations initially passivated during the SiN anneal (Fig. 5(b)), have regained recombination strength. This is likely caused by the dissolution, redistribution and re-precipitation of impurities along the grain boundaries. [2] This ‘strengthening’ of lattice dislocations would contribute to the increased  $\tau_{\text{other}}^{-1}$  observed in this wafer. Figs. 6(b) and (c) show that the degradation induced by the long anneal is less severe at the top of the brick. This is demonstrated by the fact that Fig. 6(c) exhibits the same characteristics as Fig. 5(c), though to a lesser extent.

## 5. CONCLUSIONS

Effective gettering and hydrogenation of mc-Si wafers is crucial to the production of a high efficiency mc-Si solar cells. We have shown that ‘extended’ gettering can greatly improve the  $\tau_{\text{eff}}$  of mc-Si wafers, especially if they are sourced from the top of a brick. PL imaging has shown that SiN induced hydrogenation primarily passivates lattice dislocations. However, ‘over-firing’ mc-Si wafers can lead to dissolution of metal precipitates (such as  $\beta\text{-FeSi}_2$ ) as well as negating the passivation of lattice dislocations achieved by the SiN induced hydrogenation. Wafers from the bottom of the mc-Si brick are most vulnerable to these degradation mechanisms during SiN anneals.

## ACKNOWLEDGEMENTS

The authors would like to thank the Australian Research Council for funding this work.

- 1 D. Macdonald *et al.*, J. Appl. Phys., **97** (3), 033523 (2005)
- 2 A. Buonassisi *et al.*, J. Appl. Phys., **97** (3), 074901 (2005)
- 3 J. Härkönen *et al.*, Sol. Ener. Mat., **73** (2), 125-130 (2002)

- 
- 4 P. Manshanden and L.J. Geerligs, *Sol Ener. Mat.*, **90** (7-8), 998-1012 (2006)
  - 5 I. Romijn *et al.*, 15<sup>th</sup> Workshop on Crystalline Silicon Solar Cells & Modules: Materials and Processes, Vail, Colorado, 82-85 (2005)
  - 6 W. Soppe *et al.*, in Proceedings of 16<sup>th</sup> EU PVSEC, Glasgow, Scotland (2000)
  - 7 R. Sinton and A. Cuevas, *App. Phys. Lett.*, **69** (17), 2510-2512 (1996)
  - 8 D. Macdonald *et al.*, *J. Appl. Phys.*, **95** (3), 1021-1028 (2004)
  - 9 D. Macdonald *et al.*, *App. Phys. Lett.*, **89** (14), 142107 (2006)
  - 10 T. Trupke *et al.*, *App. Phys. Lett.*, **67** (11), 044107 (2006)
  - 11 R. Sinton *et al.*, in Proceedings of 19<sup>th</sup> EU PVSEC, Paris, France (2004)
  - 12 R. A. Ramappa and W.B. Henley, *J. Electrochem. Soc.*, **144** (12), 4353-4356 (1997)
  - 13 W.B. Henley and D.A. Ramappa, *J. Appl. Phys.*, **82** (2), 589-594 (1997)
  - 14 K. Graff, *Metal Impurities in Silicon-Device Fabrication*, Vol. 24 of Springer Series in Material Science, Springer, Berlin, 2<sup>nd</sup> Revised Ed. (1999)
  - 15 D. Macdonald *et al.*, in Proceedings of the 29<sup>th</sup> IEEE Photovoltaic Specialists Conference, New Orleans, USA, 285-288 (2002)
  - 16 Z. Chen *et al.* Conference Record of the IEEE Photovoltaic Specialists, Waikoloa, Hawaii, USA, Vol. 2, 1331-1334 (1994)
  - 17 J. Tan *et al.*, *Prog. in PV*, in press (2007)
  - 18 S. Martinuzzi *et al.*, *Sol. Ener. Mat.*, **80** (3), 343-353 (2003)
  - 19 M. Rinio *et al.*, Proceedings of the 21st EU PVSEC, Dresden, Germany (2006)